Area law for magnetic domain walls in bent cylindrical nanowires

G. H. R. Bittencourt,[1] O. Chubykalo-Fesenko,[2] D. Altbir,[3] V. L. Carvalho-Santos,[1] and R. Moreno[4]

[1]*Departamento de Física, Universidade Federal de Viçosa, 36570-900 Viçosa, Brazil*
[2]*Instituto de Ciencia de Materiales de Madrid, CSIC, Cantoblanco, 28049 Madrid, Spain*
[3]*Departamento de Física, CEDENNA, Universidad de Santiago de Chile, 9170124 Santiago, Chile*
[4]*Earth and Planetary Science, School of Geosciences, University of Edinburgh, Edinburgh EH9 3FE, United Kingdom*

(Received 10 June 2022; revised 12 August 2022; accepted 12 August 2022; published xxxxxxxxxx)

The dynamics of several systems in nature occurs under some constraints and symmetries that ensure the appearance of constants of motion. In this work, we discuss the dynamics of the magnetic domain wall (DW) under the Walker regime (i.e., when its position oscillates as a function of time) in bent cylindrical magnetic nanowires (NWs) with constant curvatures. It is shown that the DW position sweeps, in relation to the curvature center, the same area for different NW curvatures. This phenomenon appears due to an exchange-driven curvature-induced interaction. The translational DW motion is accompanied by its rotation around the NW axis, leading to a periodic curvature-independent angular momentum, from which one obtains an area's law for the DW motion.

DOI: 10.1103/PhysRevB.00.004400

I. INTRODUCTION

Magnetic nanowires (NW) are nanostructures mimicking one-dimensional systems [1–3]. They have exhibited many extremely interesting phenomena [4–6], becoming a fundamental pillar for the next generation of applications at the nanoscale [7–14]. Among them, the possibility of tuning domain wall (DW) dynamics is probably the most attractive one from a technological perspective and consequently, a great deal of effort has been put in this direction [15–17]. During this undertaking, various unexpected and intriguing magnetic phenomena were reported on noncurved NWs (or nanostripes). For instance, a current-induced spin wave frequency shift was identified as a Doppler effect [18], an analogy of the Cherenkov radiation was found in magnetic domain walls emitting spin waves while moving sufficiently fast [19], or the DW width contraction for velocities close to the spin wave group velocity was shown to obey similar laws to that of the special relativity [20,21]. These examples evidence the existence of a plethora of interesting phenomena to be revealed in nanomagnetism.

Within the aim of tuning DW dynamics, the understanding of curvature-induced phenomena in magnetic NWs is an important topic in current magnetism research [22]. Curvature induces a drastic change in the role that the exchange interaction plays in DW dynamics, leading to the appearance of several interesting magnetic effects [23–31]. Among them, we can highlight the oscillatory behavior of the DW along the NW axis, similar to that corresponding to the Walker regime in straight NWs. It appears above a certain threshold for the external stimuli and reduces the DW average velocity in consonance with the Walker breakdown in faceted straight NWs [15]. Nevertheless, in contrast to their noncurved counterpart [32], this oscillatory behavior appears even for the case of circular cross-section NWs [26]. The Walker breakdown threshold field results to be proportional to the NW curvature [25,26].

In this work we demonstrate that, for the specific case of bent cylindrical NWs with constant curvature and under external magnetic fields within the Walker regime, the previously reported translational and rotational DW motions [26,27] yield a time-periodic curvature-independent angular momentum. This fact implies that the area covered by the DW when "orbiting" around the curvature center of the NW is curvature independent but exhibits a periodic time dependence. The problem is presented in Fig. 1 (based on our simulation results to be discussed below), illustrating the area law for the DW dynamics in bent NWs, where the DW sweeps equal areas in equal times, independent of the NW curvature.

II. MODEL AND RESULTS

To evidence the above statement, we analytically address the problem, corroborating our results by using micromagnetic simulations (using the finite-element software NMAG [33]). Bent NWs with constant curvature are fully described as toroidal sections with a fixed length $\ell = 1\mu$m, major radius R, minor radius $a = 15$ nm, and opening angle ψ. The relationship among these parameters is $\ell = \psi R$. The curvature is defined as $\kappa = 1/R$. In analytical calculations, R is a free parameter. The set of bent NWs considered in micromagnetic simulations is described as $\ell = \frac{2\pi R_n}{n}$, where $n \in [2, 10]$ is an integer number determining R_n, $\kappa_n = 1/R_n$, and $\psi_n = 2\pi/n$.

The magnetization inside the NW can be parameterized using the local coordinate basis, $\mathbf{m} = \sin\Omega\sin\phi\,\hat{r} + \cos\Omega\,\hat{\theta} + \sin\Omega\cos\phi\,\hat{z}$ (see Fig. 2), where M_s and $\mathbf{m} = \mathbf{M}/M_s$ are the saturation and normalized magnetization, respectively. Magnetic NWs exhibit transverse DWs (T_{dw}) up to a critical diameter $D_{CR}(M_s)$ [34]. In this work the diameter of the NWs

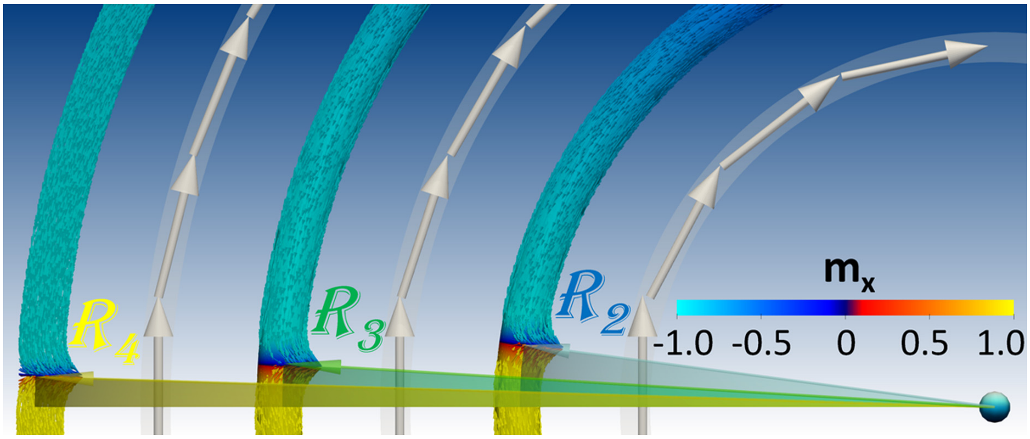

FIG. 1. Schematic representation of the area (shady regions) covered by a head-to-head transverse DW (T_{dw}) obtained from simulations for three concentric bent cylindrical nanowires with different curvatures. The sphere depicts the center of curvature for all wires. White arrows represent the applied azimuthal magnetic field with the same strength for all the NW. The magnetization is colored following its m_X component which corresponds to the in-plane vertical direction. R_2, R_3, and R_4 represent three different curvature radii.

is below this critical value, therefore we assume the existence of transversal domain walls, T_{dw}. The following ansatz is used for describing the T_{dw} profile: $\Omega = 2\arctan\{\exp[R(\theta - \theta_0)]/\delta\}$, where $R\theta_0$ defines the position of the DW center, and $\delta = \delta_W/\pi$ is the DW width (δ_W) divided by π. For our calculations, the T_{dw} is considered a rigid body, with constant shape and size. Our micromagnetic simulations support this approach. Thus, the DW dynamics can be described by the position of its center and its phase $[\phi(t)]$.

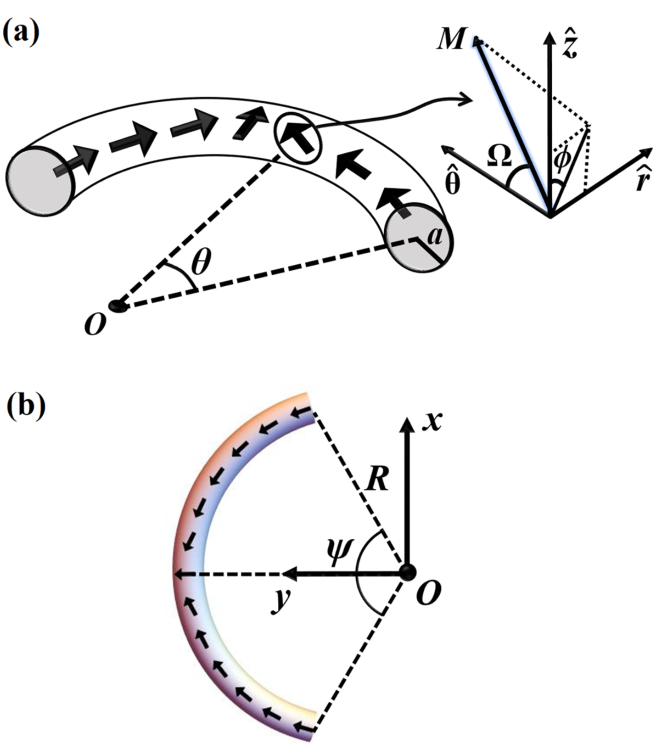

FIG. 2. (a) Domain wall profile, and local and global coordinate bases used in this work. (b) NW orientation in the Cartesian reference system and geometric parameters.

The time evolution of the magnetization is given by the Landau-Lifshitz-Gilbert (LLG) equation

$$\frac{\partial \mathbf{M}}{\partial t} = -\gamma \mathbf{M} \times \mathbf{H_{eff}} + \frac{\alpha}{M_s}\mathbf{M} \times \frac{\partial \mathbf{M}}{\partial t}, \tag{1}$$

where γ is the gyromagnetic ratio, α is the Gilbert damping parameter, and $\mathbf{H_{eff}}$ is the effective field coming from the magnetostatic, exchange, Zeeman, and anisotropy interactions. The magnetostatic effective field is obtained from the demagnetizing tensors, considering that the DW lies in an ellipsoid inside the NW. In this case, $\mathbf{H}_d = -4\pi(N_r M_r\,\hat{r} + N_\theta M_\theta\,\hat{\theta} + N_z M_z\,\hat{z})$, where N_r, N_θ, and N_z are the demagnetizing factors along the $\hat{r}$, $\hat{\theta}$, and $\hat{z}$ directions, respectively. The exchange field is $\mathbf{H}_x = (2A/M_s)\nabla^2\mathbf{m}$. For simplicity, the external magnetic field has a constant strength of $H = 11$ mT, and is chosen tangent to the NW, i.e., $\mathbf{H}_Z = H\,\hat{\theta}$ (see white arrows in Fig 1). The field strength ensures that the DW dynamics occurs under the Walker regime [26]. An azimuthal magnetic field can be experimentally addressed, for instance, from an electric current flowing perpendicular to the plane the bent NW forms. The magnetic parameters used in this work correspond to that of Permalloy, that is, the exchange stiffness and saturation magnetization are $A = 1.3 \times 10^{-11}$ J m^{-1} and $M_s = 7.95 \times 10^5$ A m^{-1}, respectively. Permalloy does not exhibit magnetocrystalline anisotropy. The domain wall width for a cylindrical Permalloy NW with diameter $d = 30$ nm is $\delta_W = 37$ nm [34]. Finally, we use the damping parameter $\alpha = 0.01$.

The DW dynamics is determined from the total torque Γ evaluated on the DW center. Specifically, the total torque corresponds to that produced by the effective field ($\Gamma_{\mathbf{eff}} = \mathbf{M} \times \mathbf{H_{eff}}$) in addition to the one coming from the damping term. The torques corresponding to the external magnetic field and the damping are straightforwardly obtained, resulting in $\mathbf{\Gamma}_H = M_s H(-\cos\phi\,\hat{r} + \mathrm{sen}\phi\,\hat{z})$ and $\mathbf{\Gamma}_\alpha = -(\alpha M_s/\gamma)(\dot{\Omega}\cos\phi\,\hat{r} + \dot{\phi}\,\hat{\theta} - \dot{\Omega}\,\mathrm{sen}\phi\,\hat{z})$, respectively. The torque originated from the dipolar effective field in the DW center is evaluated as $\mathbf{\Gamma}_d = -2\pi M_s^2 \Delta N \mathrm{sen}(2\phi)\,\hat{\theta}$, where $\Delta N = N_r - N_z$ [28]. For NWs with a circular cross section one obtains $\Delta N = 0$ and therefore, $\boldsymbol{\Gamma}_d = 0$. Finally, for bent one-dimensional (1D) systems, the most important term in the total torque on the DW consists of that produced by the exchange field, given by $\boldsymbol{\Gamma}_x = A(\frac{4\cos\phi}{R\delta} - \frac{\sin(2\phi)}{R^2})\hat{\theta}$. Under the above assumptions, the total torque can be written as

$$\boldsymbol{\Gamma}_{r,\theta,z} = \begin{bmatrix} -M_s\cos\phi\left(\frac{\alpha}{\gamma}\frac{d\Omega}{dt} + H\right) \\ -\frac{\alpha M_s}{\gamma}\frac{d\phi}{dt} + A\left(\frac{4\cos\phi}{R\delta} - \frac{\sin(2\phi)}{R^2}\right) \\ M_s\sin\phi\left(\frac{\alpha}{\gamma}\frac{d\Omega}{dt} + H\right) \end{bmatrix}. \tag{2}$$

To simplify our analysis, it is convenient to rewrite the total torque in the local system of cylindrical coordinates (see Fig. 2) as $\boldsymbol{\Gamma}_{\rho,\Omega,\phi} = \mathcal{R}\boldsymbol{\Gamma}_{r,\theta,z}$, where $\mathcal{R}$ is the rotation matrix that connects the two considered coordinate systems and $\hat{\rho}$ is a unitary radial vector. In this case, we obtain

$$\boldsymbol{\Gamma}_{\rho,\Omega,\phi} = \begin{bmatrix} 0 \\ \frac{\alpha M_s}{\gamma}\frac{d\phi}{dt} - A\left(\frac{4}{R\delta}\cos\phi - \frac{1}{R^2}\sin(2\phi)\right) \\ -M_s\left(\frac{\alpha}{\gamma}\frac{d\Omega}{dt} + H\right) \end{bmatrix}. \tag{3}$$

The substitution of the above expressions for the torques reduces the LLG [Eq. (1)] to the following system of equations for the two angles describing the DW center [see Fig. 2(a)]:

$$\frac{d\phi}{dt} = -\frac{\gamma}{M_s}\Gamma_\phi \quad \text{and} \quad \frac{d\Omega}{dt} = -\frac{\gamma}{M_s}\Gamma_\Omega\,. \tag{4}$$

Since we are evaluating the dynamics of the DW center, the linear velocity can be defined as $v = Rd\theta_0/dt = -\delta d\Omega/dt$. Therefore, after some algebra, it is possible to write the above set of equations in terms of the torque components. In this context, we obtain a system of coupled equations defining the DW velocity and phase as

$$v(t) = \frac{\gamma}{1+\alpha^2}\left[\alpha\delta H - \frac{A}{M_sR}\left(4\cos\phi - \frac{\delta}{R}\sin(2\phi)\right)\right] \tag{5}$$

$$\frac{d\phi}{dt} = \frac{\gamma}{1+\alpha^2}\left[H + \frac{\alpha A}{M_sR\delta}\left(4\cos\phi - \frac{\delta}{R}\sin(2\phi)\right)\right]. \tag{6}$$

All the geometries considered in this work fulfill that $R \gg \delta$. Thus, terms proportional to δ/R in the above equations can be neglected. Therefore, we obtain

$$v(t) \approx \frac{\gamma\delta\alpha}{(1+\alpha^2)}\left(H - \frac{4A}{RM_s\delta\alpha}\cos\phi\right) \tag{7}$$

and

$$\frac{d\phi}{dt} \approx \frac{\gamma}{1+\alpha^2}\left(H + \frac{4\alpha A}{M_sR\delta}\cos\phi\right). \tag{8}$$

The initial condition for the integration is $\phi(0) = \pi/2$ (schematically displayed in Fig. 2). That initial condition corresponds to the equilibrium state of a head-to-head T_{dw} in bent cylindrical nanowires [23] and matches with that obtained in our micromagnetic simulations.

Importantly, the term $\frac{4\alpha A}{RM_s\delta} \approx 0.1$ mT is two orders of magnitude smaller than the external applied field. Therefore, the Walker regime is obtained even for smaller external stimuli than the one considered here since the condition $\frac{4\alpha A}{RM_S\delta H} \ll 1$ holds. In Eq. (7) the damping parameters are in the denominator and thus the first term is relatively small with respect to the second one. Note that even without disregarding the second term, Eq. (8) can be integrated to yield

$$\phi(t) = 2\arctan[\eta\tanh(\omega t + \operatorname{arctanh}(\xi))], \tag{9}$$

where $\eta = \sqrt{\frac{H_W+H}{H_W-H}}$, $\xi = \sqrt{\frac{H_W-H}{H_W+H}}$, $\omega = \frac{\gamma}{2}\frac{\sqrt{H_W{}^2-H^2}}{1+\alpha^2}$, and the Walker field is $H_W = \frac{4\alpha A}{RM_s\delta}$. In the limit $\frac{4\alpha A}{RM_s\delta H} \ll 1$ we obtain

$$\phi(t) \approx \frac{\gamma H t}{1+\alpha^2} + \frac{\pi}{2}.$$

The analytical results for the DW velocity, obtained by the integration of Eqs. (7) and (8), are presented in Fig. 3(a), together with the direct micromagnetic simulations for three different curvatures (κ_n). The values of the velocity amplitude (V_{AMP}) are highlighted with dashed lines and labeled on the right axis. Clearly, the velocity amplitude increases as a function of the NW curvature. An interesting point is that the amplitude of the velocity in Eq. (7) is field independent while its frequency is not.

Figure 3(b) presents numerical and analytical results for the DW velocity amplitudes as a function of the NW curvature. Our results evidence a linear dependence between velocity and curvature. Importantly, the slope of the lines in Fig. 3(b), obtained either by a linear fit (orange line) to the numerical results (red circles) or by the analytical data (blue line), have physical units of $\mathrm{m^2\,s^{-1}}$. Therefore, Fig. 3(b) suggests the existence of an area covered in a certain amount of time which is independent of the NW curvature. This finding also directly follows from the fact that the oscillatory part of the DW velocity is proportional to $1/R$ and thus the area, covered by its radius vector, is independent from R for the same time intervals.

To explore this finding, we define the z component of the DW "angular momentum" as $L_z = \mu R v$, where μ is the DW effective mass. Assuming that the DW behaves as a particlelike structure, we can study its dynamical properties from Newton's second law. Therefore, we define

$$\Gamma_z = \frac{dL_z}{dt} = \mu R\frac{dv}{dt}. \tag{10}$$

The combination of Eqs. (2) and (7) allows us to define the DW effective mass μ as

$$\mu = \frac{\Gamma_z}{Ra_\theta(t)} = \frac{M_s^2(1+\alpha^2)}{4A\gamma^2}, \tag{11}$$

where the linear acceleration is $a_\theta(t) = \frac{dv(t)}{dt} = \frac{dv}{d\phi}\frac{d\phi}{dt}$. Thus, the z component of the angular momentum reads

$$L_z = \mu R v = \frac{\alpha\delta M_s^2 R H}{4\gamma A} - \frac{M_s}{\gamma}\cos\phi. \tag{12}$$

The first term results from the Zeeman interaction and reflects a small constant drift of the DW along the nanowire. The second term is oscillating and it is produced by the curvature-induced exchange-driven effective field. Note that due to the time dependence of the domain wall phase $\phi(t)$, the angular

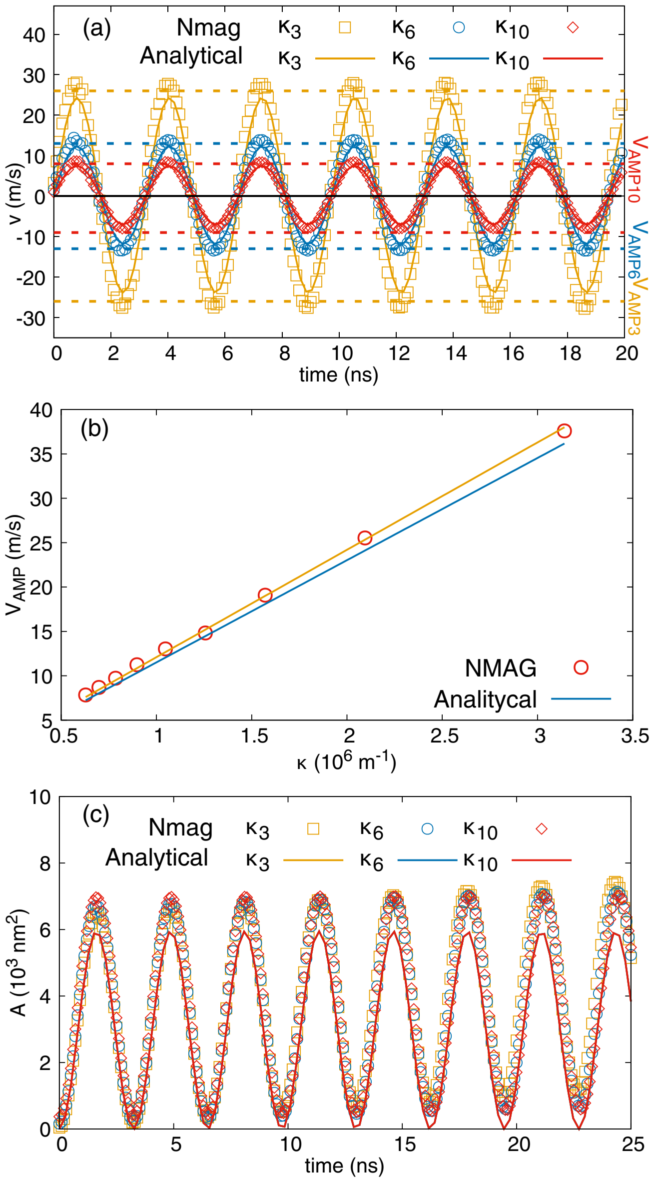

FIG. 3. (a) Time dependence of the DW velocity. Symbols and solid lines represent numerical and analytical results, respectively. The different colors stand for different NW curvatures: $\kappa_3 = 2.094$ (brown), $\kappa_6 = 1.047$ (blue), and $\kappa_{10} = 0.628$ (red) (10^6 m^{-1}). Dashed lines and labels V_{AMP} highlight the amplitude of the velocity. (b) Amplitude of the velocity vs curvature. Red circles and blue line represent numerical and analytical results, respectively. Orange line is a linear fit of the numerical results. (c) Time evolution of the area covered by the DW during its dynamics. Symbols and solid lines represent numerical and analytical results, respectively. The small linear displacement of the DW along the NW has been subtracted in our numerical results.

momentum is not conserved. However, it is a conserved quantity if one averages over the domain wall oscillating period.

Since we are interested in the dynamical component and the constant drift term in the velocity is relatively small, we only focus on the oscillatory behavior, defining the quantity $\mathscr{L}$ as

$$\mathscr{L} = L_z - \frac{\alpha\delta M_s^2 RH}{4\gamma A} = -\frac{M_s}{\gamma}\cos\left(\frac{\gamma Ht}{1+\alpha^2}+\frac{\pi}{2}\right). \quad (13)$$

Therefore, $\mathscr{L}$ is curvature independent. The rate of area that a DW covers during its dynamics is related to the angular momentum by

$$\frac{d\mathscr{A}}{dt} = \frac{R^2}{2}\frac{d\theta_0}{dt} = \frac{L_z}{2\mu} \approx \frac{\mathscr{L}}{2\mu}, \quad (14)$$

where we again disregarded the constant drift term.

Thus, although both the area and angular momentum are oscillating in time quantities, there is a simple relation between them, very analogous to that in the system with a conserved angular momentum. This fact implies that the rate of the area covered per time by the DW due to the curvature-induced exchange-driven effective interaction is independent of the curvature. This result is central for our article and is illustrated in Fig. 3(c), where analytical results are compared with direct numerical simulations.

The Newtonian-like equations of motion for the DW have the following form:

$$\mu a_R = -\frac{4A}{(1+\alpha^2)R^3}\cos^2\phi \quad (15)$$

$$\mu a_\theta = \frac{HM_s}{(1+\alpha^2)R}\sin\phi. \quad (16)$$

Equations (15) and (16) represent the centripetal-like force $(-\mu v^2/R)$ and the tangential one $(\mu dv/dt)$, respectively. The former comes from the exchange interaction, while the latter is due to the external magnetic field. These results suggest some analogy to systems moving in central potential, albeit in our case, the radial part of the potential has dependence $1/R^2$ and is oscillating in time. However, although the exchange interaction yields a central-like periodic field, one should remark that the potential is not centrosymmetric due to the nontrivial behavior of its tangential part. Low damping values ($\alpha \ll 1$) are required for the validity of the different approximations used. For this range of values, α does not play any important role in the system. Additionally, the value of the external magnetic field affects just the tangential acceleration amplitude, which increases linearly with H.

It is important to remark that the area covered at any time, as well as the maximum area evaluated at the semiperiod of oscillations, depends on the magnetic field strength

$$\mathscr{A}(t) = \frac{2A}{HM_s}\left[1-\cos\left(\frac{\gamma Ht}{1+\alpha^2}\right)\right], \quad (17)$$

which is illustrated in Fig. 3(c). Nevertheless, the average in time area covered in a half-period ($\tau/2$), i.e., $\langle\mathscr{A}\rangle = \frac{2\mathscr{A}}{\tau} = \frac{4A\gamma}{\pi M_s}$, is independent of the field strength. Clearly, it is also curvature independent. Furthermore, the value of $\langle\mathscr{A}\rangle$ matches with the amplitude value of the oscillations for the velocity (V_{AMP}) in Eq. (7) with the exception of the factor π.

III. CONCLUSIONS

In conclusion, we have reduced the dynamical LLG equation of motion for a transverse DW in bent cylindrical nanowires with a constant curvature to a Newton equation of a point nanoparticle in a centrosymmetric periodic field, produced by the exchange interaction. From the analysis of the DW angular momentum along the z axis direction, one can observe that the term corresponding to exchange interaction is curvature independent. This result allows us to obtain the area swept by the DW in relation to the center of the NW curvature. We have observed that the area covered by the DW due to the exchange-driven effective field is the same, independent of the NW curvature. This finding is associated with the increase in the DW velocity, under the Walker regime, as a function of the NW curvature. We highlight that although the swept area is independent of the NW curvature, it is oscillating in time with a constant period.

The results discussed in this work could be confused with Kepler's law for a DW "orbiting" in a circular trajectory around the curvature center. Nevertheless, the potential of interaction between the DW and an imaginary "mass center" in the system is not of the kind $V \propto 1/R$. This fact, in addition to the periodicity in the DW velocity when it displaces under the Walker regime, explain why, if we consider a constant orbit, the DW seeps different areas in the same time interval. At the same time, our results highlight that a plethora of different analogies can exist in nature, providing a rich phenomenological description of otherwise complicated physical phenomena.

We thank Prof. L. Garay for his useful discussion. R.M. acknowledges the Natural Environment Research Council (Grant No. NE/S011978/1). O.C.F. acknowledges Grant No. PID2019-108075RB-C31/AEI/10.13039/501100011033 from the Spanish Ministry of Science and Innovation. V.L.C.-S. and G.H.R.B. acknowledge the Brazilian agencies CNPq (Grant No. 302084/2019-3) and the Coordenação de Aperfeiçoamento de Pessoal de 279 Nivel Superior - Brasil (CAPES) - Finance Code 001. D.A. acknowledges the Chilean Basal Center Cedenna under Grant No. AFB180001 and Fondecyt 1220215.

[1] A. Fert and L. Piraux, Magnetic nanowires, J. Magn. Magn. Mater. **200**, 338 (1999).

[2] M. Vazquez, *Magnetic Nano- and Microwires* (Elsevier, New York, 2020)

[3] M. Staňo and O. Fruchart, *Handbook of Magnetic Materials* (Elsevier, New York, 2018), Chap. 3, pp. 155–267.

[4] V. V. Slastikov and C. Sonnenberg, Reduced models for ferromagnetic nanowires, IMA J. Appl. Math. **77**, 220 (2012).

[5] R. Wieser, U. Nowak, and K. D. Usadel, Domain wall mobility in nanowires: Transverse versus vortex walls, Phys. Rev. B **69**, 064401 (2004).

[6] C. Bran, E. Berganza, J. A. Fernandez-Roldan, E. M. Palmero, J. Meier, E. Calle, M. Jaafar, M. Foerster, L. Aballe, A. Fraile Rodriguez, R. P. del Real, A. Asenjo, O. Chubykalo-Fesenko, and M. Vazquez, Magnetization ratchet in cylindrical nanowires, ACS Nano **12**, 5932 (2018).

[7] D. A. Allwood, G. Xiong, M. D. Cooke, C. C. Faulkner, D. Atkinson, N. Vernier, and R. P. Cowburn, Submicrometer ferromagnetic not gate and shift register, Science **296**, 2003 (2002).

[8] S. S. P. Parkin, M. Hayashi, and L. Thomas, Magnetic domain-wall racetrack memory, Science **320**, 190 (2008).

[9] L. Atzori, A. Iera, and G. Morabito, The Internet of Things: A survey, Computer Networks **54**, 2787 (2010).

[10] M. R. Zamani Kouhpanji and B. J. H. Stadler, Magnetic nanowires for nanobarcoding and beyond, Sensors **21**, 4573 (2021).

[11] N. Rossi, B. Gross, F. Dirnberger, D. Bougeard, and M. Poggio, Magnetic force sensing using a self-assembled nanowire, Nano Lett. **19**, 930 (2019).

[12] T. Maurer, F. Ott, G. Chaboussant, Y. Soumare, J.-Y. Piquemal, and G. Viau, Magnetic nanowires as permanent magnet materials, Appl. Phys. Lett. **91**, 172501 (2007).

[13] H.-J. Cui, J.-W. Shi, B. Yuan, and M.-L. Fu, Synthesis of porous magnetic ferrite nanowires containing Mn and their application in water treatment, J. Mater. Chem. A **1**, 5902 (2013).

[14] A. Espejo, F. Tejo Lazo, N. Vidal, and J. Escrig, Nanometric alternating magnetic field generator, Sci. Rep. **7**, 4736 (2017).

[15] D. Altbir, J. M. Fonseca, O. Chubykalo-Fesenko, R. M. Corona, R. Moreno, V. L. Carvalho-Santos, and Y. P. Ivanov, Tuning domain wall dynamics by shaping nanowires cross-sections, Sci. Rep. **10**, 21911 (2020).

[16] C. Bran, J. A. Fernandez-Roldan, R. P. del Real, A. Asenjo, O. Chubykalo-Fesenko, and M. Vazquez, Magnetic configurations in modulated cylindrical nanowires, Nanomaterials **11**, 600 (2021).

[17] S. Dwivedi and S. Dubey, On the evolution of transverse domain walls in biaxial magnetic nanowires, Mater. Today: Proc. **4**, 10555 (2017), International Conference on Recent Trends in Engineering and Material Sciences (ICEMS-2016), March 17–19, 2016, Jaipur, India.

[18] V. Vlaminck and M. Bailleul, Current-induced spin-wave doppler shift, Science **322**, 410 (2008).

[19] M. Yan, A. Kákay, C. Andreas, and R. Hertel, Spin-Cherenkov effect and magnonic Mach cones, Phys. Rev. B **88**, 220412(R) (2013).

[20] L. Caretta, S.-H. Oh, T. Fakhrul, D.-K. Lee, B. H. Lee, S. K. Kim, C. A. Ross, K.-J. Lee, and G. S. D. Beach, Relativistic kinematics of a magnetic soliton, Science **370**, 1438 (2020).

[21] Takayuki Shiino, Se-Hyeok Oh, Paul M. Haney, Seo-Won Lee, Gyungchoon Go, Byong-Guk Park, and Kyung-Jin Lee, Antiferromagnetic domain wall motion driven by spin-orbit torques, Phys. Rev. Lett. **117**, 087203 (2016).

[22] D. Sheka, A perspective on curvilinear magnetism, Appl. Phys. Lett. **118**, 230502 (2021).

[23] K. V. Yershov, V. P. Kravchuk, D. D. Sheka, and Y. Gaididei, Curvature-induced domain wall pinning, Phys. Rev. B **92**, 104412 (2015).

[24] V. Kravchuk, Influence of Dzialoshinskii-Moriya interaction on static and dynamic properties of a transverse domain wall, J. Magn. Magn. Mater. **367**, 9 (2014).

[25] K. V. Yershov, V. P. Kravchuk, D. D. Sheka, and Y. Gaididei, Curvature and torsion effects in spin-current driven domain wall motion, Phys. Rev. B **93**, 094418 (2016).

[26] R. Cacilhas, C. I. L. de Araujo, V. L. Carvalho-Santos, R. Moreno, O. Chubykalo-Fesenko, and D. Altbir, Controlling domain wall oscillations in bent cylindrical magnetic wires, Phys. Rev. B **101**, 184418 (2020).

[27] R. Moreno, V. L. Carvalho-Santos, A. P. Espejo, D. Laroze, O. Chubykalo-Fesenko, and D. Altbir, Oscillatory behavior of the domain wall dynamics in a curved cylindrical magnetic nanowire, Phys. Rev. B **96**, 184401 (2017).

[28] G. H. R. Bittencourt, R. Moreno, R. Cacilhas, S. Castillo-Sepúlveda, O. Chubykalo-Fesenko, D. Altbir, and V. L. Carvalho-Santos, Curvature-induced emergence of a second critical field for domain wall dynamics in bent nanostripes, Appl. Phys. Lett. **118**, 142405 (2021).

[29] K. V. Yershov, V. P. Kravchuk, D. D. Sheka, O. V. Pylypovskyi, D. Makarov, and Y. Gaididei, Geometry-induced motion of magnetic domain walls in curved nanostripes, Phys. Rev. B **98**, 060409(R) (2018).

[30] T. Blachowicz and A. Ehrmann, Magnetic elements for neuromorphic computing, Molecules **25**, 2550 (2020).

[31] T. Blachowicz and A. Ehrmann, Magnetization reversal in bent nanofibers of different cross sections, J. Appl. Phys. **124**, 152112 (2018).

[32] M. Yan, A. Kákay, S. Gliga, and R. Hertel, Beating the Walker Limit with Massless Domain Walls in Cylindrical Nanowires, Phys. Rev. Lett. **104**, 057201 (2010).

[33] T. Fischbacher, M. Franchin, G. Bordignon, and H. Fangohr, A systematic approach to multiphysics extensions of finite-element-based micromagnetic simulations: Nmag, IEEE Trans. Magn. **43**, 2896 (2007).

[34] R. Moreno, V. L. Carvalho-Santos, D. Altbir, and O. Chubykalo-Fesenko, Detailed examination of domain wall types, their widths and critical diameters in cylindrical magnetic nanowires, J. Magn. Magn. Mater. **542**, 168495 (2022).